Simulation of Two-Dimensional Contaminant Transport With Isoparametric Hermitian Finite Elements

MARTINUS T. VAN GENUCHTEN AND GEORGE F. PINDER

Department of Civil Engineering, Princeton University, Princeton, New Jersey 08540

EMIL O. FRIND

Department of Earth Sciences, University of Waterloo, Waterloo, Ontario, Canada

A deformed isoparametric Hermitian element can be used in the simulation of two-dimensional contaminant transport. The degree of freedom arising from the cross derivative may be eliminated in the Galerkin-type finite element formulation, reducing the computational effort per node. Two example problems demonstrate that the Hermitian element gives results which are comparable to those obtained with the zero-order continuous cubic element but requires 25–40% fewer degrees of freedom, depending on the geometrical description of the problem.

INTRODUCTION

Numerical solutions of the convective-dispersive transport equation have received considerable attention recently owing to the increased interest in contaminant and heat transport simulation. The partial differential equation governing two-dimensional transport of a conservative ionic species in an incompressible flow field can be written as

$$L(c) = \frac{\partial}{\partial x}\left(D_{xx}\frac{\partial c}{\partial x}\right) + \frac{\partial}{\partial x}\left(D_{xy}\frac{\partial c}{\partial y}\right) + \frac{\partial}{\partial y}\left(D_{yx}\frac{\partial c}{\partial x}\right) - \frac{\partial}{\partial y}\left(D_{yy}\frac{\partial c}{\partial y}\right) - \frac{\partial}{\partial x}(V_x c) - \frac{\partial}{\partial y}(V_y c) - \frac{\partial c}{\partial t} = 0 \qquad (1)$$

where

c solute concentration, ML^{-3};
D dispersion coefficient, L^2T^{-1};
t time, T;
V mass average velocity, LT^{-1}.

The purpose of this paper is to examine a method for the numerical solution of (1) by using isoparametric finite elements in conjunction with first-order continuous Hermitian basis functions.

THEORETICAL DEVELOPMENT

Galerkin Approximation

The approximate integral equations which provide the foundation for the finite element approach can be generated by using a Galerkin formulation. In this approach the unknown function c is approximated by using a finite series of the form

$$c(x, y, t) \approx \hat{c}(x, y, t) = \sum_{j=1}^{n} a_j(t)\phi_j(x, y) \qquad (2)$$

where the $\phi_j(x, y)$ are basis functions chosen beforehand such that they satisfy the essential boundary conditions imposed on (1) and the $a_j(t)$ are undetermined coefficients. In the present analysis these coefficients become the values of c, $\partial c/\partial x$, $\partial c/\partial y$, and $\partial^2 c/(\partial x\,\partial y)$ at the nodal locations. The Galerkin method requires that the residual arising out of the substitution of $\hat{c}$ for c in (1) be orthogonal to each of the n basis functions ϕ_j. From the definition of orthogonal functions this can be expressed as

$$\int_A L(\hat{c})\phi_i(x, y)\,dA = 0 \qquad i = 1, 2, \cdots, n \qquad (3)$$

where A is the domain over which the integration is performed. Expansion of (3) provides n equations in the n unknowns $a_j(t)$. Because it is the intention of this paper to focus primarily on the form of the approximating function $\hat{c}$ and the geometric transformations inherent in the isoparametric formulation, the reader is referred to other work, such as that of *Pinder* [1973], for a specific discussion of the coefficient matrices obtained from (3).

Basis Functions

As is true of zero-order continuous polynomials, the Hermitian first-order continuous basis functions can be generated in two ways. In an approach analogous to the development of 'Lagrangian' elements the two-dimensional bases are obtained simply as the product of the well-known one-dimensional expressions. In the local (ξ) coordinate system (Figure 1) the one-dimensional Hermitian basis functions are written [*Oden*, 1972, p. 54] as

$$\phi_0^1 = -\tfrac{1}{4}(\xi + \xi_0)^2(\xi\xi_0 - 2) \qquad (4a)$$

$$\phi_1^1 = \tfrac{1}{4}\xi_0(\xi + \xi_0)^2(\xi\xi_0 - 1) \qquad (4b)$$

where $\xi_0 = \pm 1$. The coefficients $a_j(t)$ in (2) are now the nodal values of the concentration and its first derivatives.

The basis functions in two dimensions (ξ, η) are obtained by multiplying (4a) by (4b):

$$\phi_{00}^1 = \tfrac{1}{16}(\xi + \xi_0)^2(\xi\xi_0 - 2)(\eta + \eta_0)^2(\eta\eta_0 - 2) \qquad (5a)$$

$$\phi_{10}^1 = -\tfrac{1}{16}\xi_0(\xi + \xi_0)^2(\xi\xi_0 - 1)(\eta + \eta_0)^2(\eta\eta_0 - 2) \qquad (5b)$$

$$\phi_{01}^1 = -\tfrac{1}{16}(\xi + \xi_0)^2(\xi\xi_0 - 2)\eta_0(\eta + \eta_0)^2(\eta\eta_0 - 1) \qquad (5c)$$

$$\phi_{11}^1 = \tfrac{1}{16}\xi_0(\xi + \xi_0)^2(\xi\xi_0 - 1)\eta_0(\eta + \eta_0)^2(\eta\eta_0 - 1) \qquad (5d)$$

where $\xi_0 = \pm 1$ and $\eta_0 = \pm 1$.

The series approximation for c as expressed through (2) may

Paper number 6W0935.

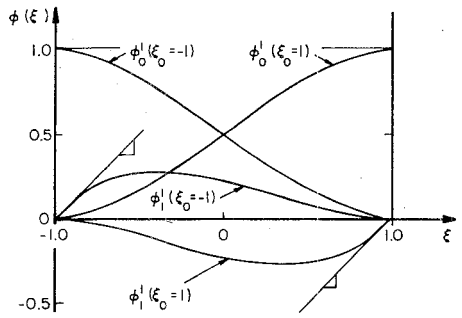

Fig. 1. First-order continuous Hermitian basis functions [after *Zienkiewicz*, 1971].

now be written as

$$c \approx \hat{c} = \sum_{j=1}^{4} \left\{ \phi_{00j}{}^{1} C_j + \phi_{10j}{}^{1} \frac{\partial C_j}{\partial \xi} + \phi_{01j}{}^{1} \frac{\partial C_j}{\partial \eta} + \phi_{11j}{}^{1} \frac{\partial^2 C_j}{\partial \xi \, \partial \eta} \right\} \tag{6}$$

The elements of the unknown vector are hence the concentration C, its first derivatives $\partial C/\partial \xi$ and $\partial C/\partial \eta$, and its cross derivative $\partial^2 C/(\partial \xi \, \partial \eta)$, each being evaluated at a node. The cross derivative should be included for completeness of the two-dimensional expansion [*Brebbia and Connor*, 1974]. Inclusion of this term leads to a continuous normal derivative at interelement boundaries for rectangular elements but does not in general do so for distorted elements [*Frind*, 1977]. Fortunately, an accurate solution of the convective-dispersive equation does not require a priori that the normal derivatives be continuous at the interelement boundaries. Because there will be a 25% reduction in the number of degrees of freedom per element (i.e., 12 rather than 16) when the cross derivative can be eliminated, it is important to obtain an expansion which does not include the cross derivative. Such an approach to formulating the two-dimensional basis functions is now considered.

Let the cubic interpolation function for the element of Figure 2*a* be given by

$$\hat{c} = \sum_{j=1}^{12} a_j(t) \omega_j(\xi, \eta) \tag{7a}$$

where the a_j are the nodal values of the concentration and the ω_j are the cubic basis functions, given by [*Ergatoudis et al.*, 1968]

$$\omega_j = \tfrac{1}{32}(1 + \xi\xi_0)(1 + \eta\eta_0)[-10 + 9(\xi^2 + \eta^2)] \tag{7b}$$

$$\xi_0 = \pm 1 \qquad \eta_0 = \pm 1$$

$$\omega_j = \tfrac{9}{32}(1 - \xi^2)(1 + 9\xi\xi_0)(1 + \eta\eta_0) \tag{7c}$$

$$\xi_0 = \pm \tfrac{1}{3} \qquad \eta_0 = \pm 1$$

$$\omega_j = \tfrac{9}{32}(1 - \eta^2)(1 + 9\eta\eta_0)(1 + \xi\xi_0) \tag{7d}$$

$$\xi_0 = \pm 1 \qquad \eta_0 = \pm \tfrac{1}{3}$$

Differentiating (7*a*) yields

$$\frac{\partial \hat{c}}{\partial \xi} = \sum_{j=1}^{12} a_j \frac{\partial \omega_j}{\partial \xi} \tag{8a}$$

$$\frac{\partial \hat{c}}{\partial \eta} = \sum_{j=1}^{12} a_j \frac{\partial \omega_j}{\partial \eta} \tag{8b}$$

If (8*a*) and (8*b*) are evaluated at the corners of the element and if we require that $a_1 = C_1$, $a_4 = C_2$, $a_7 = C_3$, and $a_{10} = C_4$ (see Figure 2), then the remaining a_j can be obtained in terms of C and its derivatives. Substituting the resulting values of a_j into (7*a*) yields

$$\begin{aligned}
\hat{c} = {} & \tfrac{1}{8}(1 - \xi)(1 - \eta)(2 - \xi - \eta - \xi^2 - \eta^2) C_1 \\
& + \tfrac{1}{8}(1 + \xi)(1 - \eta)(2 + \xi - \eta - \xi^2 - \eta^2) C_2 \\
& + \tfrac{1}{8}(1 + \xi)(1 + \eta)(2 + \xi + \eta - \xi^2 - \eta^2) C_3 \\
& + \tfrac{1}{8}(1 - \xi)(1 + \eta)(2 - \xi + \eta - \xi^2 - \eta^2) C_4 \\
& + \tfrac{1}{8}(1 - \xi^2)(1 - \xi)(1 - \eta) \, \partial C_1/\partial \xi \\
& - \tfrac{1}{8}(1 - \xi^2)(1 + \xi)(1 - \eta) \, \partial C_2/\partial \xi \\
& - \tfrac{1}{8}(1 - \xi^2)(1 + \xi)(1 + \eta) \, \partial C_3/\partial \xi \\
& + \tfrac{1}{8}(1 - \xi^2)(1 - \xi)(1 + \eta) \, \partial C_4/\partial \xi \\
& + \tfrac{1}{8}(1 - \eta^2)(1 - \xi)(1 - \eta) \, \partial C_1/\partial \eta \\
& + \tfrac{1}{8}(1 - \eta^2)(1 + \xi)(1 - \eta) \, \partial C_2/\partial \eta \\
& - \tfrac{1}{8}(1 - \eta^2)(1 + \xi)(1 + \eta) \, \partial C_3/\partial \eta \\
& - \tfrac{1}{8}(1 - \eta^2)(1 - \xi)(1 + \eta) \, \partial C_4/\partial \eta
\end{aligned} \tag{9}$$

Equation (9) can be written as

$$\hat{c} = \sum_{j=1}^{4} \left\{ \phi_{00j} C_j + \phi_{10j} \frac{\partial C_j}{\partial \xi} + \phi_{01j} \frac{\partial C_j}{\partial \eta} \right\} \tag{10a}$$

where

$$\phi_{00j} = (1/8)(1 + \xi\xi_0)(1 + \eta\eta_0)(2 + \xi\xi_0 + \eta\eta_0 - \xi^2 - \eta^2) \tag{10b}$$

$$\phi_{10j} = -(\xi_0/8)(1 - \xi^2)(1 + \xi\xi_0)(1 + \eta\eta_0) \tag{10c}$$

$$\phi_{01j} = -(\eta_0/8)(1 - \eta^2)(1 + \xi\xi_0)(1 + \eta\eta_0) \tag{10d}$$

We denote the functions ϕ_{00j}, ϕ_{10j}, and ϕ_{01j} as serendipity-type Hermitian basis functions. These functions can also be derived from the Lagrangian type (16 degrees of freedom) by introducing an appropriate difference approximation for the cross-derivative terms. A graphical representation of these functions is given in Figure 3.

Isoparametric Transformation

Because (9) and (10) are expressed in the local coordinates ξ and η, they apply only over the local element of Figure 4*a*. The transformation from the local coordinate system to the global (x, y) system can be accomplished by using the same basis functions as appear in (10). The transformation which makes the square of Figure 4*a* into the deformed element of Figure 4*b* is given by

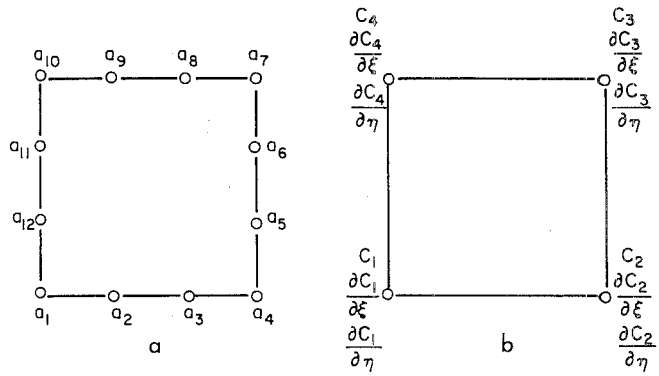

Fig. 2. Nodal arrangements for (*a*) zero-order continuous cubic and (*b*) Hermitian elements.

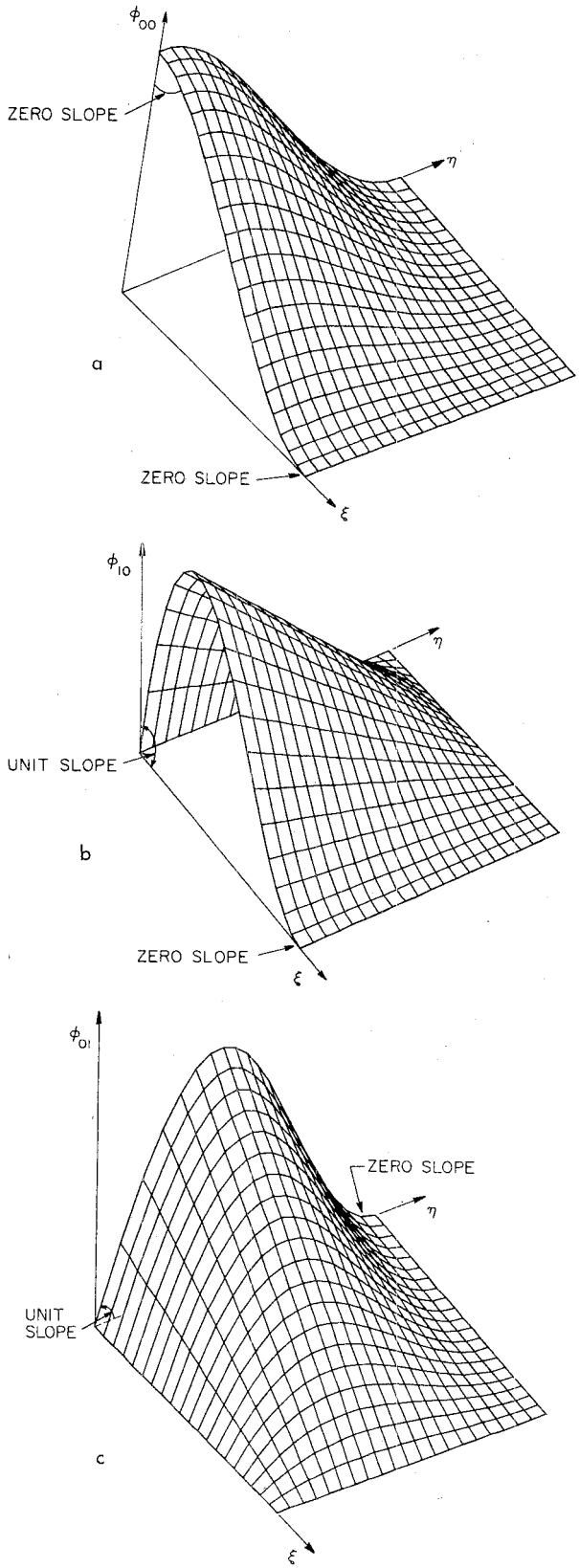

Fig. 3. Two-dimensional Hermitian basis functions.

$$x(\xi, \eta) = \sum_{j=1}^{4} \left\{ \phi_{00j} X_j + \phi_{10j} \frac{\partial X_j}{\partial \xi} + \phi_{01j} \frac{\partial X_j}{\partial \eta} \right\} \tag{11a}$$

$$y(\xi, \eta) = \sum_{j=1}^{4} \left\{ \phi_{00j} Y_j + \phi_{10j} \frac{\partial Y_j}{\partial \xi} + \phi_{01j} \frac{\partial Y_j}{\partial \eta} \right\} \tag{11b}$$

where X_j, Y_j, $\partial X_j/\partial \xi$, $\partial Y_j/\partial \xi$, $\partial X_j/\partial \eta$, and $\partial Y_j/\partial \eta$ are the nodal x-y coordinates and their derivatives with respect to the ξ-η coordinate system. The nodal derivatives can be defined in terms of the geometric properties of the distorted element. For example, for node 1 (Figure 4) we have

$$\frac{\partial X_1}{\partial \xi} = \frac{L_1}{2} \cos \alpha_1 \qquad \frac{\partial Y_1}{\partial \xi} = \frac{L_1}{2} \sin \alpha_1$$
$$\frac{\partial X_1}{\partial \eta} = \frac{L_4}{2} \cos \beta_1 \qquad \frac{\partial Y_1}{\partial \eta} = \frac{L_4}{2} \sin \beta_1 \tag{12}$$

where L_1 and L_4 are the lengths of sides 1 and 4 (Figure 4). These side lengths can be evaluated by making use of a formula of the form

$$L = \int_{-1}^{1} \left[\left(\frac{\partial x}{\partial \xi} \right)^2 + \left(\frac{\partial y}{\partial \xi} \right)^2 \right]^{1/2} d\xi \tag{13}$$

The derivatives $\partial x/\partial \xi$ and $\partial y/\partial \xi$ in (13) may be obtained by differentiating (11) with respect to ξ and are evaluated at $\eta = -1$ and $\eta = +1$ for sides 1 and 3, respectively. (For sides 2 and 4, ξ and η have to be interchanged.) Because L appears not only on the left-hand side of the equation but also through (11) and (12) in the argument of the integral, it is clear that iteration is necessary in order to obtain the correct side lengths. This iteration usually converges rapidly. For the two examples considered in this study, less than five iterations were required to obtain answers correct to within 0.005%.

Because the unknowns in this study are the nodal values of the concentration C and its derivatives $\partial C/\partial x$ and $\partial C/\partial y$, the approximation (10a) must be rewritten in terms of these unknowns. From the chain rule we have

$$\frac{\partial C}{\partial \xi} = \frac{\partial C}{\partial x} \frac{\partial X}{\partial \xi} + \frac{\partial C}{\partial y} \frac{\partial Y}{\partial \xi}$$
$$\frac{\partial C}{\partial \eta} = \frac{\partial C}{\partial x} \frac{\partial X}{\partial \eta} + \frac{\partial C}{\partial y} \frac{\partial Y}{\partial \eta} \tag{14}$$

Substituting (14) into (10a) and rearranging give

$$\hat{c} = \sum_{j=1}^{4} \left\{ \phi_{0j} C_j + \phi_{xj} \frac{\partial C_j}{\partial x} + \phi_{yj} \frac{\partial C_j}{\partial y} \right\} \tag{15}$$

where

$$\phi_{0j} = \phi_{00j}$$
$$\phi_{xj} = \phi_{10j} \frac{\partial X_j}{\partial \xi} + \phi_{01j} \frac{\partial X_j}{\partial \eta} \tag{16}$$
$$\phi_{yj} = \phi_{10j} \frac{\partial Y_j}{\partial \xi} + \phi_{01j} \frac{\partial Y_j}{\partial \eta}$$

When deformed isoparametric quadrilateral finite elements are used, the integrals that arise out of the elementwise integration of (3) must be evaluated with numerical methods. The required integrations are carried out directly on the square element in the local coordinates between the limits -1 and $+1$, using a 4×4 Gaussian quadrature scheme. In this method the area element dA in (3) has to be replaced by

$$dA = \det [J] \, d\xi \, d\eta \tag{17}$$

where the Jacobian J is defined by

$$[J] = \begin{bmatrix} \partial x/\partial \xi & \partial y/\partial \xi \\ \partial x/\partial \eta & \partial y/\partial \eta \end{bmatrix}$$

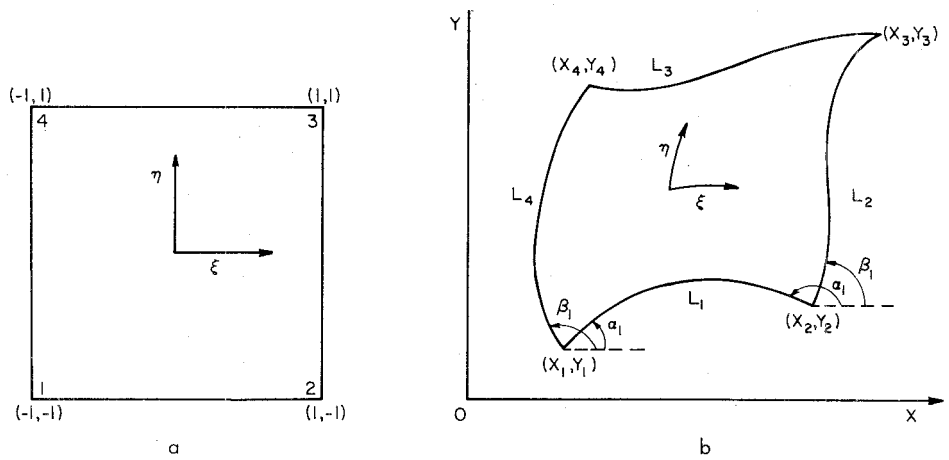

Fig. 4. Deformed isoparametric Hermitian elements in (*a*) local and (*b*) global coordinates.

The basis function derivatives $\partial\phi/\partial x$ and $\partial\phi/\partial y$ that appear in the integrals are easily evaluated by using

$$\begin{Bmatrix} \partial\phi/\partial x \\ \partial\phi/\partial y \end{Bmatrix} = [J]^{-1} \begin{Bmatrix} \partial\phi/\partial\xi \\ \partial\phi/\partial\eta \end{Bmatrix} \tag{18}$$

The Jacobian can be evaluated numerically by expressing it in terms of the nodal x-y coordinates [*Ergatoudis et al.*, 1968] and the nodal gradients $\partial X/\partial\xi$, $\partial Y/\partial\xi$, etc.

Once the basis functions are defined and the isoparametric formulation is completed, (1) and (3) can be combined with (15) and (17) to give a set of n ordinary differential equations in n unknowns. The finite element formulation from this point on proceeds as outlined by *Pinder* [1973]. Central finite differences are used to approximate the time derivatives, and a matrix solver which takes advantage of the banded nature of the coefficient matrices is used for solution of the final set of equations.

APPLICATIONS

Two examples are considered here to demonstrate the use of deformed isoparametric Hermitian elements in the simulation of two-dimensional contaminant transport. Solutions are obtained for both the Hermitian cubic and the zero-order continuous cubic elements, so that a comparison can be made of both the accuracy and the efficiency of the two elements. The geometries of the examples are chosen such that the numerical solutions can be compared with available analytical solutions.

Example 1

In this example, solute is transported through a rectangular region as depicted in Figure 5. The elements inside the slab are distorted as shown in the figure, and the following initial and boundary conditions are adopted:

$$c = 0 \qquad (x, y) \notin \Gamma_1 \qquad t = 0 \tag{19a}$$

$$c = 1 \qquad (x, y) \in \Gamma_1 \qquad t \geq 0 \tag{19b}$$

$$\partial c/\partial n = 0 \qquad (x, y) \in \Gamma_2, \Gamma_3, \Gamma_4 \qquad t \geq 0 \tag{19c}$$

where n represents the direction normal to the boundary. When no rotation is present (i.e., $\alpha = 0$), the problem becomes one dimensional, and the solute distribution inside the slab is given by

$$C = \tfrac{1}{2}\,\mathrm{erfc}\,[(x - Vt)/(4Dt)^{1/2}] + \tfrac{1}{2}\exp(Vx/D)\,\mathrm{erfc}\,[(x + Vt)/(4Dt)^{1/2}] \tag{20}$$

where V and D are the solute velocity and the dispersion coefficient, respectively, for one-dimensional transport. For a rotation of $\alpha°$ the velocities and dispersion coefficients in (1) are related to V and D by

$$V_x = V\cos\alpha \qquad V_y = V\sin\alpha \tag{21a}$$

$$D_{xx} = D_{yy} = D \qquad D_{xy} = D_{yx} = 0 \tag{21b}$$

Since the physical system remains the same irrespective of the coordinate system adopted, it is clear that (20) may also be used to describe the solute distribution inside the rectangle of Figure 5.

Two provisions must be made in the numerical formulation before the problem can be simulated correctly. First, it should be noted that it is not immediately clear what values $\partial c/\partial x$ and $\partial c/\partial y$ should have at the inlet position Γ_1 at the start of the simulation ($t = 0$). If we assume that these values are initially zero, an error is introduced, as is readily demonstrated for the one-dimensional case as follows. If we assume C_2 and $\partial C_2/\partial\xi$ to be zero ($\xi = 1$), the initial concentration inside the element is given by (see Figure 1)

$$\hat{c}_{e=1} = C_1\phi_0^1 + (\partial C_1/\partial\xi)\phi_1^1 \tag{22}$$

When $C_1 = 1$ and $\partial C_1/\partial\xi$ is assumed to be zero, the simulated initial distribution will not be zero but will follow the curve ϕ_0^1 ($\xi_0 = -1$) of Figure 1. However, by choosing $\partial C_1/\partial\xi = -3$ it is readily shown that [*van Genuchten*, 1976]

$$\int_{-1}^{1} \hat{c}_{e=1}\, d\xi = 0 \tag{23}$$

By satisfying (23) the initial concentration as averaged over the first element is still zero, and the material balance of the solute will be correct. Similar problems arise when other basis functions are used. For the cubic element, for example, an average zero initial concentration may be obtained by forcing the concentration at the midside nodes to be slightly negative. No such correction, however, is possible for linear elements, since by specifying $C_1 = 1$ at the first node and $C_2 = 0$ at the second node the concentration inside the element will be fixed and will be determined by a straight line from boundary Γ_1 to the first interelement node.

A second problem may be encountered in the correct formulation of boundary condition (19*c*). In the case of Hermitian

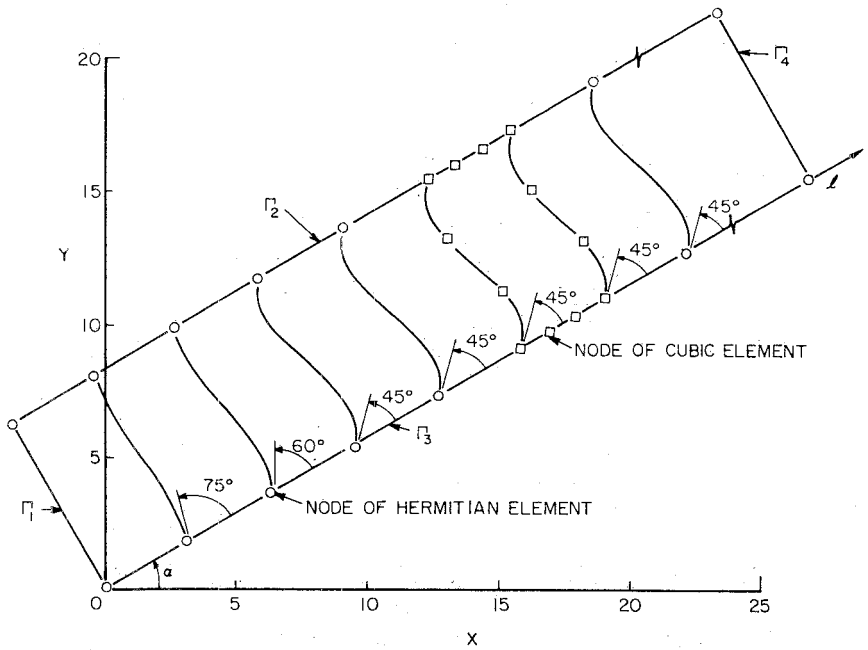

Fig. 5. Schematic representation of nodal arrangement for finite element solution of example 1.

basis functions this condition is easily satisfied by expanding the unknowns $\partial C/\partial x$ and $\partial C/\partial y$ into normal ($\partial C/\partial n$) and tangential ($\partial C/\partial T$) components as follows:

$$\frac{\partial C}{\partial n} = -\sin\gamma\,\frac{\partial C}{\partial x} + \cos\gamma\,\frac{\partial C}{\partial y} \qquad (24a)$$

$$\frac{\partial C}{\partial T} = \cos\gamma\,\frac{\partial C}{\partial x} + \sin\gamma\,\frac{\partial C}{\partial y} \qquad (24b)$$

where γ is the angle between the boundary side considered and the x coordinate direction. Boundary condition (19c) will be satisfied by requiring that $\partial C/\partial n$ in (24a) be zero.

Parameter values for example 1 were taken from the work of *Peaceman and Rachford* [1962] and are as follows: node spacing of 182.9/50, or 3.658 cm; velocity (V in (21a)) of 0.01411 cm/s; dispersion coefficient (D in (21b)) of 0.001 cm²/s; time step of 50 s; and total elapsed time of 3250 s (65 time steps). Simulation results for this example are shown in Figures 6–8.

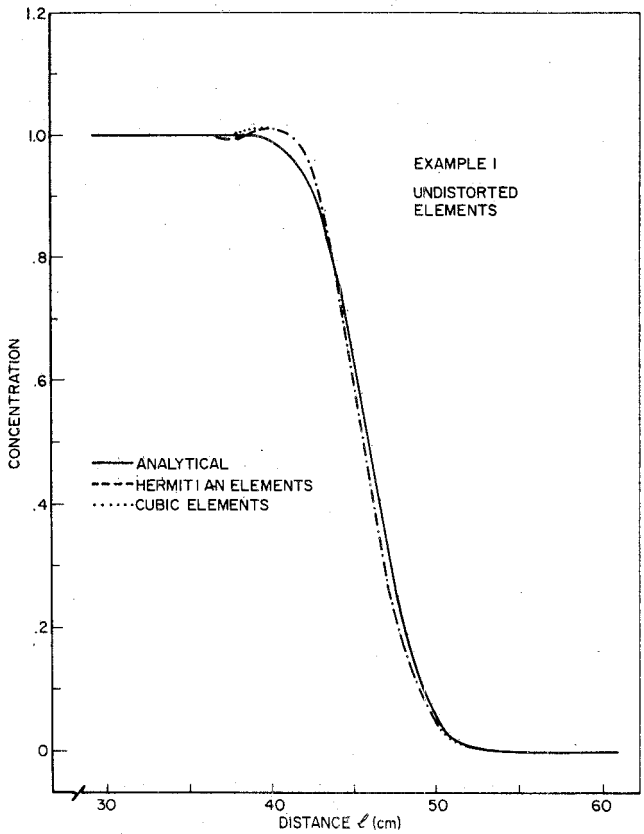

Fig. 6. Concentration profiles obtained by using undistorted zero-order continuous cubic and Hermitian elements.

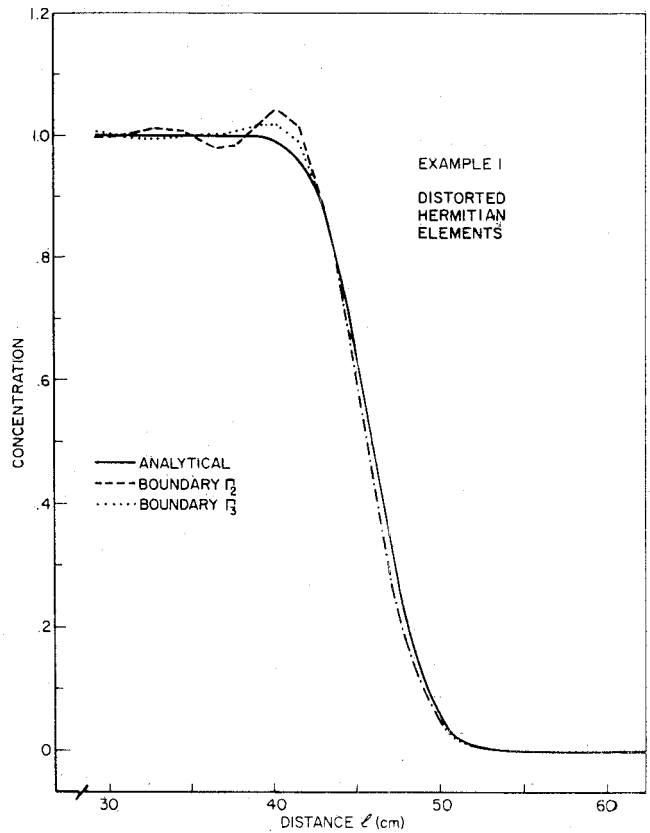

Fig. 7. Concentration profiles obtained by using distorted Hermitian elements.

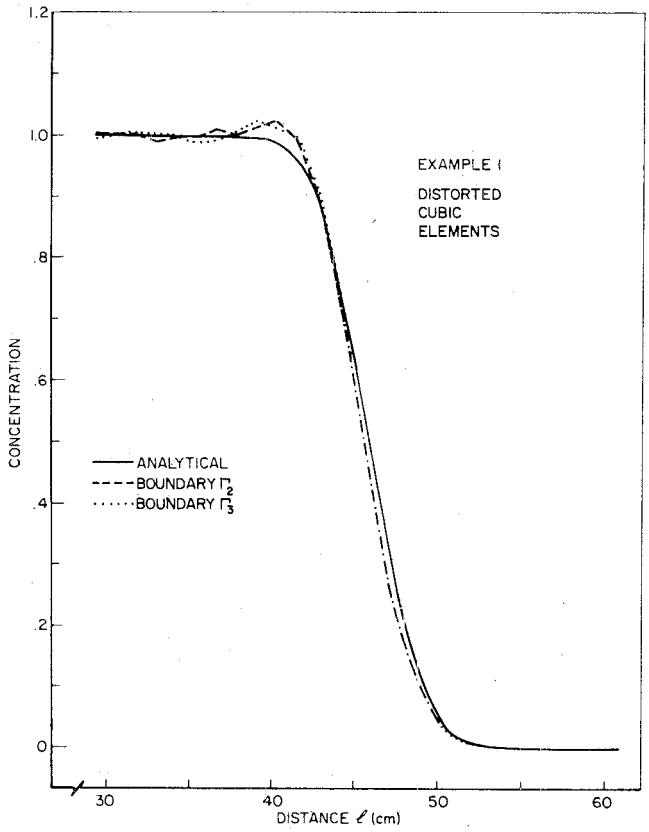

Fig. 8. Concentration profiles obtained by using distorted zero-order continuous cubic elements.

Figure 6 gives the analytical solution and the results obtained for the undistorted zero-order continuous and Hermitian elements. Both the Hermitian and the zero-order continuous cubic elements produce approximately the same results and agree closely with the analytical solution. Some deviations from the analytical solution are apparent at around 40 cm, a result that is typical of the problem encountered when the mass transport equation is solved for large velocities and relatively small dispersion coefficients [*Pinder*, 1974]. This behavior is often referred to as 'overshoot.' Results for the distorted elements are shown in Figures 7 and 8. Figure 7 compares the Hermitian element solution with the analytical solution. Distributions for both the upper (Γ_2) and the lower (Γ_3) boundary are plotted in the figure. Figure 8 gives similar results for the zero-order continuous cubic element, using the same distorted elements as were used for the Hermitian case. Note that the numerical results are different along boundaries Γ_2 and Γ_3 in both figures. This may be expected, since the elements are distorted differently when these boundaries are approached from the inside. Again, basically the same results are obtained for the two elements, although the oscillations for the Hermitian element are somewhat more severe than those for the zero-order continuous cubic element. The results for the one-dimensional case (Figure 6) are only slightly better than those for the two-dimensional simulations.

An important consideration in comparing the relative merits of the two elements is the number of degrees of freedom required to solve a particular problem, i.e., the number of equations which have to be solved during the numerical calculations. For the one-dimensional case, two additional degrees of freedom are introduced for each additional Hermitian element, compared with three degrees of freedom for the zero-order continuous cubic element. Hence 50% more equations must be solved when zero-order continuous cubic elements rather than Hermitian elements are used to solve the one-dimensional convective-dispersive equation. For the two-dimensional problem sketched in Figure 5 this ratio is 6:8 in favor of the Hermitian element. Note, however, that only one row of elements was used to describe the geometry in this problem; when additional rows are considered, the above ratio ultimately becomes 3:5 in favor of the Hermitian element.

Example 2

In this example the combined effects of radial convection and dispersion are considered. A contaminant source, for example, a contaminated recharging well, is located at the center of a confined homogeneous isotropic aquifer. Because of symmetry, only a pie-shaped wedge of 22.5° is considered in the finite element formulation (Figure 9). The radial velocity V_r of the incompressible fluid is given by

$$V_r = Q/(2\pi\rho r) \tag{25}$$

where ρ is the density of the fluid and Q is the amount of fluid transported across any circle per unit time. The boundary value problem describing the contaminant distribution during

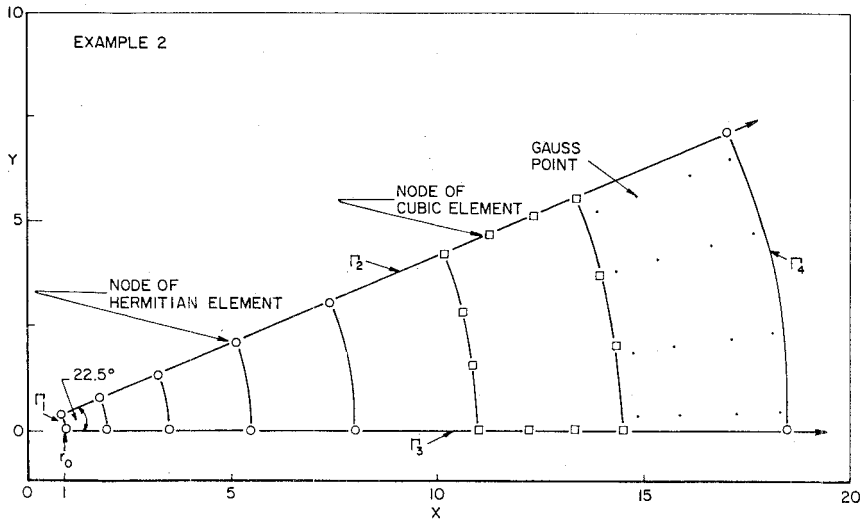

Fig. 9. Schematic representation of nodal arrangement for finite element solution of example 2.

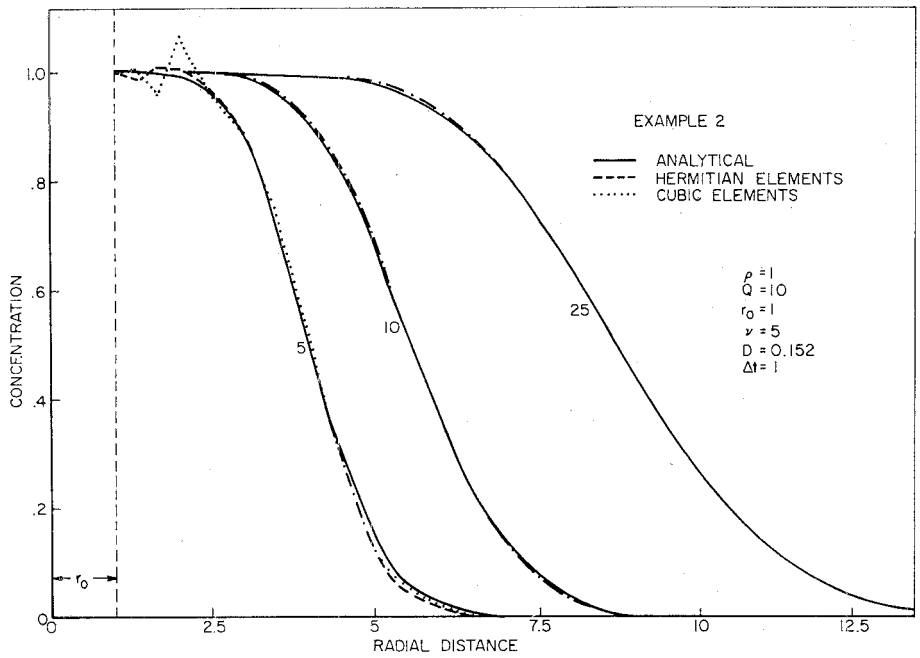

Fig. 10. Concentration profiles obtained by using zero-order continuous cubic and Hermitian elements.

steady radial flow may be stated in radial coordinates as

$$D\frac{\partial^2 c}{\partial r^2} + \left(\frac{D}{r} - V_r\right)\frac{\partial c}{\partial r} - \frac{\partial c}{\partial t} = 0 \tag{26}$$

$$\begin{aligned} c &= 0 \qquad t = 0 \qquad r > r_0 \\ c &= 1 \qquad t \geq 0 \qquad r = r_0 \\ \partial c/\partial r &= 0 \qquad t \geq 0 \qquad r \to \infty \end{aligned} \tag{27}$$

The analytical solution for this problem is given by *Carslaw and Jaeger* [1959, p. 390] as

$$c = 1 + \frac{2}{\pi}\left(\frac{r}{r_0}\right)^{\nu}\int_0^{\infty} e^{-u^2 Dt}\,\frac{J_\nu(ur)Y_\nu(ur_0) - Y_\nu(ur)J_\nu(ur_0)}{u[J_\nu^2(ur_0) + Y_\nu^2(ur_0)]}\,du \tag{28}$$

where J_ν and Y_ν are Bessel functions of the first and second kind, respectively, and ν is defined by

$$\nu = Q/(4\pi D\rho) \tag{29}$$

By using radial coordinates $x = r\cos\theta$ and $y = r\sin\theta$ it is readily shown that the concentration distribution in the aquifer can also be described by (1), provided the following relations are satisfied:

$$\begin{aligned} V_x &= V_r\cos\theta \qquad V_y = V_r\sin\theta \\ D_{xx} &= D_{yy} = D \qquad D_{xy} = D_{yx} = 0 \end{aligned} \tag{30}$$

At least two approaches are possible to evaluate the variable velocities V_x and V_y. One possibility is to expand the velocities in terms of the basis functions and the nodal values of V_x and V_y (and its derivatives if Hermitian functions are used [e.g., *Pinder et al.*, 1973]). A somewhat simpler approach follows. Since the velocities are determined by (25) and (30), the only problem left is to evaluate these expressions at the Gauss points (X_G, Y_G), which are required for the numerical integration of the integrals appearing in the coefficient matrices. The Gauss points are easily expressed in terms of the global coordinate system by using (11). Figure 9 shows the location of the Gauss points in an arbitrary element. The velocities V_x and V_y are then computed by using (25) and (30) together with the following relations:

$$\begin{aligned} \theta &= \tan^{-1}(Y_G/X_G) \\ r &= (X_G^2 + Y_G^2)^{1/2} \end{aligned} \tag{31}$$

Simulation results for example 2 are presented in Figure 10. Results for both the Hermitian and the cubic elements are given and compared with the analytical solution. Values of the parameters Q, D, r_0, ρ, ν, and Δt are given in the figure. The relatively small integer value 5 was chosen for ν to facilitate the evaluation of the integral appearing in (28). In contrast to the first example the same concentration distributions were obtained for boundaries Γ_2 and Γ_3 because the elements of the present problem are distorted in exactly the same fashion along Γ_2 and Γ_3. The figure shows excellent agreement between the numerical and analytical solutions. Some oscillations are present during the first few time steps, especially for the zero-order continuous cubic element. This may be due to very high velocities in the elements nearest to the well. Because the velocities decrease rapidly with increasing radial distance, the oscillations disappear rather quickly. After 10 time steps (t = 10) the numerical and analytical results are essentially identical.

Conclusions

The two examples considered show that the Hermitian element gives results in the solution of the convective-dispersive equation that are comparable to those obtained with the zero-order continuous cubic element. The Hermitian element, however, generates 25–40% fewer degrees of freedom and is therefore more efficient than the zero-order cubic element. A substantial part of the saving was achieved by eliminating the cross derivative $\partial^2 C/(\partial x\,\partial y)$ from the solution, which is feasible when continuous normal derivatives at the interelement boundaries are not required.

Acknowledgment. This work was supported in part by funds obtained from the Solid and Hazardous Waste Research Division, Envi-

ronmental Protection Agency, Municipal Environmental Research Laboratory, Cincinnati, Ohio (EPA grant R803827-01).

REFERENCES

Brebbia, C. A., and J. J. Connor, *Fundamentals of Finite Element Techniques,* Butterworths, London, 1974.

Carslaw, H. S., and J. C. Jaeger, *Conduction of Heat in Solids,* 2nd ed., Oxford University Press, New York, 1959.

Ergatoudis, I., B. M. Irons, and O. C. Zienkiewicz, Curved isoparametric, 'quadrilateral' elements for finite element analysis, *Int. J. Solids Struct., 4,* 31–42, 1968.

Frind, E. O., An isoparametric Hermitian element for the solution of field problems, *Int. J. Numer. Methods Eng., 10,* in press, 1977.

Oden, J. T., *Finite Elements of Nonlinear Continua,* McGraw-Hill, New York, 1972.

Peaceman, D. W., and H. H. Rachford, Jr., Numerical calculation of multi-dimensional miscible displacement, *Soc. Petrol. Eng. J., 2,* 327–339, 1962.

Pinder, G. F., A Galerkin–finite element simulation of groundwater contamination on Long Island, New York, *Water Resour. Res., 9*(6), 1657–1669, 1973.

Pinder, G. F., Progress in simulation of contaminant transport in porous media, *Proc. Annu. Amer. Water Resour. Conf., 19,* 223–239, 1974.

Pinder, G. F., E. O. Frind, and S. S. Papadopulos, Functional coefficients in the analysis of groundwater flow, *Water Resour. Res., 9*(1), 222–226, 1973.

van Genuchten, M. T., On the accuracy and efficiency of several numerical schemes for solving the convective-dispersive equation, paper presented at International Conference on Finite Elements in Water Resources, Water Resour. Program, Princeton Univ., Princeton, N. J., July 12–16, 1976.

Zienkiewicz, O. C., *The Finite Element Method in Engineering Science,* McGraw-Hill, New York, 1971.

(Received April 6, 1976;
revised November 15, 1976;
accepted December 16, 1976.)